國立清華大學生命科學院

系統神經科學研究所

碩士論文

節細胞在 RCS 大鼠視網膜退化過程晚期之形態與生理特性

Morphology and Physiology of Retinal Ganglion Cells in Royal College of Surgeons Rats at Later Stages of Degeneration

指導教授： 焦傳金 博士 (Dr. Chuan-Chin Chiao)

研 究 生： 黃玄軒 (Wen-Hsuan Huang)

學 號： g9780542

中華民國一百年一月

摘　要

因感光細胞退化而造成失明的人類先天色素性視網膜炎中，視網膜神經網絡會出現重塑現象。在利用 RCS 大鼠作為人類色素性視網膜炎的模式動物之研究報告指出，因感光細胞退化晚期所造成之重塑會使內核層細胞與節細胞發生嚴重重組現象。現今色素性視網膜炎的治療方法均是基於殘存神經細胞的功能仍然完好，忽略退化晚期的重塑現象。然而，因為鮮少有針對退化晚期視網膜節細胞特性的研究，故本篇研究希望以形態與電生理的方式描述視網膜節細胞於退化晚期之特性。研究利用出生後 331 至 418 天、526 至 575 天的 RCS 大鼠與兩種正常大鼠（SD 及 LE），比較其視網膜節細胞在形態是否有差異，另外在 RCS 及 SD 大鼠上也進行視網膜節細胞的生理特性初探。在形態研究上是利用顯微注射 Neurobiotin 染劑的方式去評估節細胞樹突結構與連結模式。在電生理的實驗中，我們與交通大學吳重雨教授合作視網膜晶片計畫，記錄 SD 大鼠的節細胞對光刺激與電刺激的反應，也記錄 RCS 大鼠的節細胞對電刺激的反應，其中電刺激的來源是藉由雷射光去引發下視網膜感光二極體矽晶片所產生。雖然我們並沒有發現 RCS 大鼠的節細胞能對下視網膜晶片的電刺激產生反應，但在節細胞的形態方面，我們卻發現包括節細胞樹突的總長度、樹突分支點的數量、樹突節點的出現率以及染劑連通其他細胞的模式在重塑晚期的 RCS 大鼠中都相較於正常大鼠有顯著差異。這項發現顯示節細胞的形態在退化晚期的 RCS 大鼠中已經出現明顯改變，因此這項特性也說明在治療退化晚期色素性視網膜炎的策略上，不能夠假設殘存的視網膜節細胞其功能仍然完好。

關鍵字：視網膜重塑，色素性視網膜炎，樹突形態

ABSTRACT

The retinal remodeling is known in a human inherited disease, retinitis pigmentosa (RP), which leads to the loss of vision caused by photoreceptor degeneration. It has been reported in the Royal College of Surgeons (RCS) rat which is one of animal models for studying human retinitis pigmentosa that the degenerated photoreceptors cause a dramatic reorganization of retina, including the inner nuclear layer and the ganglion cell layer, at later stages in the RCS rat. At present treatments for restoring vision in RP founded on the intact properties of remaining neurons, and the remodeling of retinal degeneration at later stages were neglected. However, the morphological features of retinal ganglion cells (RGCs) in the RCS rat at later stages of degeneration have not been carefully studied. Therefore, the goals of this study were to characterize the properties of RGCs at later stages in morphology and electrophysiology. In the present study, we characterized morphological properties of RGCs in two aged groups of RCS rats (P331-418 and P526-575) and two strains of normal rats (SD and LE). In addition, examination of the physiological properties of RGCs in SD and RCS rats was also attempted. The responses of RGCs upon light and electrical stimulations in SD rats, and those upon electrical stimulation in RCS rats were recorded. Microinjection with Neurobiotin was used to assess the dendritic morphologies and coupling patterns of RGCs. In collaboration with Prof. CY Wu (National Chiao Tung University) in retinal prosthesis program, the electrical stimulation was provided by activating a silicone-based microphotodiode array with a 532 nm laser from the

subretinal side. Although we did not find RGC responses upon electrical stimulation in the RCS rat, the morphological features of RGCs, including total dendritic length, number of branching points, appearance of dendritic beads, and tracer coupling patterns in the RCS rats were significantly different from those in the normal rats. The finding indicates that RGCs in the RCS rat may undergo significant changes during the retinal remodeling at later stages of degeneration. This also suggests that the strategy of treating RP at later stages cannot assume intact RGCs.

Key words: retinal remodeling, retinitis pigmentosa, dendritic morphology

誌　謝

感謝有幸能完成小小的研究，並寫成著作與大家分享，即便在巨人的肩膀上還爬得不夠高，但還是期望這樣的研究成果能夠幫助其他研究走得更遠、更高。每當閱讀那些新發現或是過往研究，總會思考著與研究相同年代的那時的我，到底是為何揮霍了這些光陰；在我出生前的年代的人們，又是如何在艱困的環境下進行研究？對於科學研究的這份熱情和謙卑態度，或許是不夠積極的；然而，在指導教授 焦傳金老師這兩年半的指導下，不僅是在實驗、研究方向和論文修改給予極大幫助，另外在人生思考以及研究態度方面也給予許多鼓勵；感謝老師不吝惜犧牲寶貴時間給予指導，以及總是帶著正面積極的精神渲染大家，讓我們更能克服沮喪和挫敗。另外本篇研究還要感謝擔任口試委員的林伯剛醫師和楊恩誠老師，給予許多相關知識、實驗與論文上的寶貴建議。

在清華的時光中，感到最幸運的就是遇到妳們：非常感謝雅婷學姐帶領懵懵懂懂的我進入實驗以及相關paper的閱讀和討論，學姐對於實驗細心負責的態度、克服實驗困難的行動力以及批判性的邏輯思考一直是我要好好效法學習的；芸潔學姐在實驗上幫助、鼓勵以及生活上的支持；懿欣學姐的好吃料理以及從澳洲寄來的鼓勵話語；雅茜學姐協助我渡過實驗難關並給予許多建言與支持；李珣學姐在生活和實驗上的分享以及給予的支持；冠陵在學習上的討論和貼心的鼓勵；怡廷在實驗卡關時的討論、幫助與默默型的關心；宜蓉、詩蓉、思羽、翼鳴、俐瑋、介恆等學弟妹的支持鼓勵。此外，特別感謝宏雅學姐及尹芃，無論是在夜深了的實驗室或是晚飯時間一路以來的陪伴，除了在實驗上給予很大的幫助外，妳們的關心與體諒，支持著我走往接下來的路。很榮幸能與妳們相識，從妳們身上學

到許多人生應有的態度，也讓我更加看清自己的缺點。

感謝慶三總是提醒著我要不斷思考，給予我適當的批判與鼓勵。非常感謝爸爸媽媽平時的關心、支持以及鼓勵；感謝姐姐總是與我討論困惑及難處，給予我許多建議和經驗分享；感謝弟弟給予心靈上的支持。還要感謝這段日子被我麻煩到的大家，多謝大家的幫忙。最後，謝謝林伯剛醫師提供的RCS大鼠，還有動物房照料的大鼠、兔子們，感謝你們的犧牲。

當學習得越多，就越加覺得自己渺小；我相信這段日子裡的學習，只是神經領域的冰山一角，感謝老師帶領我進入這有趣的領域，感謝許多前人的辛勤研究，感謝在這領域拓展中的研究人員們，感謝這些研究要讓人類更接近真理的心。

TABLE OF CONTENTS

摘　要 i

ABSTRACT ii

誌　謝 iv

CHAPTER 1. INTRODUCTION 1

1.1 Retinal circuitry 1

1.2 Loss of vision by photoreceptor degeneration 2

1.3 Strategies for restoring of vision 4

1.4 Goals and approaches 6

CHAPTER 2. MATERIALS AND MATHODS 8

2.1 Animals 8

2.2 Retina preparation 9

2.3 Microinjection 10

2.4 Light and electrical stimulations 11

2.5 Extracellular recording 12

2.6 Image acquisition 13

2.7 RGC tracing and classification 13

2.8 Data analysis 14

CHAPTER 3. RESULTS 15

3.1 Morphological classification of RGCs in dystrophic RCS rats and normal rats 15

3.2 Dendritic features of RGCs in dystrophic RCS rats and normal rats 16

3.3 Tracer coupling pattern and dendritic beads of RGCs in dystrophic RCS rats and normal rats 17

3.4 Cell number in the GCL and the IPL width in dystrophic RCS rats and normal rats 18

3.5 Responses of RGCs upon light and electrical stimulations in normal rats 18

3.6 Responses of RGCs upon electrical stimulation in RCS rats 20

CHAPTER 4. DISCUSSION 21

4.1 Changes of the RGC morphology in the RCS rat at the later degeneration stages 21

4.2 Abnormal communication of RGCs in the RCS rats 22

4.3 Responses of RGCs upon electrical stimulation in normal rats 23

4.4 Responses of RGCs upon electrical stimulation in the RCS rats 24

4.5 Summary 25

REFERENCES 26

TABLES 33

FIGURES 35

SUPPLEMENTARY MATERIALS 46

CHAPTER 1

INTRODUCTION

1.1 Retinal circuitry

About one hundred years ago, the great Spanish anatomist Santiago Ramon y Cajal (1852-1934) elaborately described the structure of the retina. Retina is composed of five major classes of neurons, and has a five-layered organization. The five classes of retinal neurons are: photoreceptors (rods and cones), bipolar cells, ganglion cells, horizontal cells, and amacrine cells, and the five layers include: the outer nuclear layer (ONL), the outer plexiform layer (OPL), the inner nuclear layer (INL), the inner plexiform layer (IPL), and the ganglion cell layer (GCL). The ONL, INL, and GCL are places where the cell somata are located, and the OPL and IPL are areas where synaptic connections are made (Wassle, 2004). Moreover, just behind the neural retina is the retinal pigment epithelium (RPE), which is a monolayer of pigmented cells close to the outer segment of photoreceptors (Strauss, 2005).

In 1892, Cajal indicated that photoreceptors, bipolar and ganglion cells are involved in the vertical pathways and horizontal and amacrine cells are involved in the lateral interactions. The major visual signals are processed from photoreceptors to ganglion cells. The first step of seeing takes place when photoreceptors (rods and cones) convert light information into electrical signal. The visual pigments (rhodopsin and opsin) resided in the photoreceptor outer segments (POS) are light-sensitive, and the initial phototransduction cascade is started by a light-induced

conformational change of these proteins. These visual cycle and the photoreceptor functions are maintained by RPE. Upon light stimulation, rods and cones reduce glutamate releasing at their synaptic terminals (rod spherules and cone pedicles), because of their hyperpolarization of membrane potential. The postsynaptic neurons express different kinds of glutamate receptors (GluRs): rod bipolar and ON cone bipolar cells express metabotropic glutamate receptors (mGluR6) (Masu et al., 1995) and are depolarized under light stimulation, while OFF cone bipolar cells express the ionotropic GluRs (iGluRs: AMPA or KA receptors) (DeVries, 2000) and are hyperpolarized by light. The ON and OFF bipolar cells make synapses with ON and OFF ganglion cells, respectively. Ganglion cells are the final output neurons which send the processed signal from retina to the brain via a bundle of ganglion cell axons (optic nerve). The horizontal and amacrine cells can modulate the responses of ganglion cells via the lateral inhibition pathways (Masland, 2001; Wassle, 2004).

1.2 Loss of vision by photoreceptor degeneration

Age-related macular degeneration (AMD) and retinitis pigmentosa (RP) are two major types of retinopathies in human. AMD is ranked as third leading visual impairment or blindness with the incidence rate of 0.6-3% in peoples over 50 years old (Jager et al., 2008). AMD is caused from atrophy of RPE (dry form) that has few symptoms in the early stage, and about 10 percent patients may have choroidal neovascularization (wet form). These fragile blood vessels

could separate photoreceptors and RPE. Without nutrients supplied from RPE, photoreceptors ultimately die and degenerate (de Jong, 2006). RP is a general name which includes retinal dystrophies with photoreceptor loss and POS accumulation (Hamel, 2006). It is a common hereditary retinal degeneration (RD) disease and affects 1 in 4000 millions of people worldwide (Hartong et al., 2006). RP is inherited as an autosomal-dominant (ad), autosomal-recessive (ar), or X-linked trait, and involves greater than 45 identified genes (Hartong et al., 2006) which are mostly rhodopsin related genes (Jones & Marc, 2005). In the early stage of RP patients, night blindness is the main symptom, but it is usually neglected (Hamel, 2006).

Even though these two diseases have different mechanisms, they cause common abnormal photoreceptor degeneration and retinal remodeling (Fariss et al., 2000; Sullivan et al., 2007). To understand mechanisms and remodeling process of RD, several specific animal models have been analyzed. In 1938, an inherited retinal degeneration in rats was first discovered (Bourne et al., 1938). In 1965, Sidman inbreeded them and named the strain Royal College of Surgeons (RCS) rat (Sidman et al., 1965). The RCS rat is the common animal model similar to human phenotype of arRP, whereas some transgenic models like P23H and S334ter rats are of adRP (Jones & Marc, 2005). Changes in the retina of the RCS rat were evident that photoreceptor nuclei decreased at 19-22 days of age (Bourne *et al.*, 1938; Dowling & Sidman, 1962), bipolar cell processes became shorter (Wang et al., 2005a), horizontal cells disorganized in 3 months (Chu et al., 1993), and synapses were found outside the normal plexiform layers (Marc *et al.*,

2003; Jones & Marc, 2005). Based on several anatomical and physiological studies, retinas have dramatic deafferented and circuitry change in different RD species (Eisenfeld *et al.*, 1984; Marc *et al.*, 2003; Cuenca *et al.*, 2005; Jones & Marc, 2005; Wang *et al.*, 2005a; Marc *et al.*, 2007; Barhoum *et al.*, 2008; Machida *et al.*, 2008; Ray *et al.*, 2010). In general, retinal remodeling proceeds through three phases. Phase 1 is photoreceptor stress: retina neurons lost the input of photoreceptors, outer segment shortening, photoreceptors deconstruction, bipolar and horizontal cells retraction, and Müller cells hypertrophy. Phase 2 is photoreceptor death: complete loss of photoreceptors, the distal fibrotic glial seal and the formation of Müller cell distal processes. Phase 3 is neuronal remodeling: neurite fascicle and microneuroma are formed in early phase 3, and neuronal migration, cell death, IPL rewiring and laminar deformation occur in late phase 3. Detailed mechanisms underlying this remodeling and functions of the remaining neurons are still unclear (Marc *et al.*, 2003; Jones & Marc, 2005).

1.3 Strategies for restoring vision

According to those studies of RD, several therapeutic strategies are developed: (1) Primary gene therapy is an approach to prevent the primary gene defects, and about 146 gene loci associated with RD have been identified (Wright et al., 2010). However, primary gene therapy is restricted at early age interventions. (2) Transplantation and stem cell therapies. In 1976, the experiment of chimeric rats (pink-eyed RCS strain with pigmented normal rat) indicated that

photoreceptors juxtaposed to normal RPE cells were rescued (Mullen & LaVail, 1976). In 1990, the subretinal injection of bFGF can delay photoreceptor degeneration (Faktorovich et al., 1990). Other methods like the RPE transplantation (Wang *et al.*, 2005b; Wang *et al.*, 2008), survival factor injection (Perry et al., 1995) and progenitor transplantation (MacLaren et al., 2006) were also studied. (3) A newly secondary gene therapy to recover retinal function is the expression photosensitive proteins directly in remaining retinal neurons (Lagali et al., 2008; Lin et al., 2008; Thyagarajan et al., 2010). (4) Retinal prostheses have been developed for decades. In 1755, French physician Charles Le Roy induced blind to sense light by using electrical charge through the eye, a remarkable experiment revealed a possibility to rescue hundreds and thousands of blinds from endless dark. In 1990s, several researchers developed two different approaches for retinal prosthesis: epiretinal and subretinal stimulations (Zrenner, 2002), by implanting a stimulating device to corresponding positions in the eyes. Implanting the chip on the surface of the inner retina and stimulating ganglion cells directly is called epiretinal implant. A successful prosthetic design requires proper settings of many electrical stimulus parameters like electrode size, current, duration etc., where many groups seeked to increase the resolution of retinal prostheses. Chichilinsky and co-workers have developed a multielectrode array that could provide temporally precision and spatially specific responses at low-threshold in macaque monkey retina and P23H rat retina (Sekirnjak et al., 2008; Sekirnjak et al., 2009). The subretinal implant is positioned between bipolar cell layer and retinal pigment epithelium for compensating

photoreceptor degeneration directly. The greatest advantage of subretinal stimulation is that the remaining retinal circuitry could evoke responses of RGCs by using photodiodes-derived current from the chip. The subretinal implant can also reduce the surgical risk compared to the epiretinal implant. Zrenner and his groups investigated the long term stability and biocompatibility of subretinal implants, and they found no significant side effect of subretinal implants on retinal function (Zrenner et al., 1999).

1.4 Goals and approaches

RD symptoms are less noticeable in the early stage of patients. Most strategies of restoring vision are based on remaining retinal neuron circuits, thus the timing of these treatments is very important. Many studies focus on degeneration and remodeling in RD of the ONL and OPL, but the properties of RGCs are still unclear. Whether the gradual loss of photoreceptors in RD animals would influence the structure and function of RGCs is the key question that we are addressing in this study. The primary goal of this study is to examine the morphology and physiology of RGCs in the RD model at later stages of degeneration.

In this study, we used microinjection with Neurobiotin to assess dendritic morphologies of RGCs and in collaboration with Prof. CY Wu (National Chiao Tung University) to characterize the responses of RGCs upon electrical stimulation from solar-cell based subretinal chip. Previous studies only investigated responses of RGCs under light or electrical stimulation in mammalian

retinas separately (Jensen *et al.*, 2005; Fried *et al.*, 2006; Jensen & Rizzo, 2006; Shyu *et al.*, 2006; Jensen & Rizzo, 2007), thus lacking the comparison between responses of identical retinal ganglion cells upon light and electrical stimulations. It is crucial to compare the responses of RGCs upon light and electrical stimulation for retinal prosthesis design. Our goals were to examine the morphological characteristics of RGCs in normal rats and in RCS rats at their later stages of degeneration and measure light and electrical responses of the same RGCs in normal rats.

CHAPTER 2

MATERIALS AND METHODS

2.1 Animals

The RCS rats which show inherited retinal dystrophy (Dowling & Sidman, 1962; Sidman *et al.*, 1965) were used in this study. The RCS rat is known to have a hereditary mutation of the Mertk gene that is mainly expressed in the RPE of the retina (D'Cruz et al., 2000; Gal et al., 2000). The altered RPE due to the non-functional MerTK protein fails to remove the shed POS by phagocytosis (LaVail et al., 1972), which results the POS debris accumulation in the subretinal space (LaVail & Battelle, 1975). These excessive POS debris may potentially cause cytotoxicity and produce free radicals, which in turn damage photoreceptors (D'Cruz et al., 2000). Degeneration of photoreceptors in the RCS rat begins approximately at 21 days of age (Bourne et al., 1938). These rats show disappearance of the ERG b-wave at 2-3 months after birth, and their rod cells are completely degenerated at postnatal day (P)100 (LaVail & Battelle, 1975). Furthermore, loss of photoreceptor inputs has been known to cause retinal circuitry remodeling which onsets at P270 in the RCS rat (Marc *et al.*, 2003; Jones & Marc, 2005). In the present study, all RCS rats (n=17) at later stages of degeneration (Group 1: P331-418, Group 2: P526-575) were obtained from the lab of Dr. PK Lin (Taipei Veterans General Hospital). The common laboratory rats, the albino Sprague-Dawley (SD) and pigmented Long-Evans (LE) rats (from BioLasco Taiwan Co., Ltd and the National Laboratory Animal Center, respectively), were

used as normal controls. The ages of SD (n=4) and LE rats (n=3) were P54-85 and P45-46, respectively. All rats were maintained on a 12 hour light/dark cycle in the NTHU animal facility.

2.2 Retina preparation

A day prior of enucleation, the rats were anesthetized with intramuscular injection of a mixture of 75 mg/kg ketamine (Imalgène 1000; Merial, France) and 15 mg/kg xylazine (Rompun solution 2%; Bayer, Germany) and locally application of 3-4 drops of topical anesthetic proparacaine hydrochloride 0.5% ophthalmic solution Alcaine (Alcon-Couvreur, Belgium), before intraocularly injecting 1.2 μl of 4', 6-diamidino-2-phenylindole (DAPI; Sigma, Germany) to label cell nuclei. The rats were allowed to recover. On the experimental day, the rats were used without dark adaption for microinjection experiment. For electrophysiological study, the rats were dark adapted for at least one hour. The rats were deeply anesthetized with intramuscular injection of a mixture of ketamine (75 mg/kg) and xylazine (15 mg/kg). The eyeballs were dissected under dim red light and hemisected behind the ora serrata. The anterior parts of eyes and vitreous were removed carefully, and the posterior parts were immersed in the modified AMES medium (120 mM NaCl, 3.1 mM KCl, 0.5 mM KH_2PO_4, 1.2 mM $MgSO_4$, 1.15 mM $CaCl_2$, 6.0 mM D-glucose) containing 23 mM $NaHCO_3$ (Ames & Nesbett, 1981). The retinas were gently separated from the retinal pigment epithelium. The anesthetized rats were euthanized with CO_2. All animals were handled according to the Association for Research in Vision and

Ophthalmology statement for the use of animals in ophthalmic and vision research, and the protocol was approved by the institutional animal care and use committee.

Four cuts were made to flatten the retina. The flattened retinas were placed photoreceptor-side down on the silicone-based subretinal chip for physiology experiment, or on filter papers for microinjection experiment (Millipore, Ireland). The preparations were transferred to a custom-made chamber attached to a stage of fluorescence microscope (Axioskop 2 FS Plus; Zeiss, Germany) and continuously superfused with heated AMES medium (34-37°C) at a flow rate 2-2.5 ml/ min.

2.3 Microinjection

RGCs were injected with dyes using micropipettes that were pulled by a programmable Flaming-Brown P97 puller (Sutter Instrument, Novato, CA) from thick-wall borosilicate glass capillaries with filament (o.d.=1.0 mm, i.d.=0.5 mm; Sutter Instrument). The micropipettes were filled with 4% or 8% Neurobiotin (Vector Laboratories, Burlingame, CA) and 2% Lucifer Yellow (Sigma) in 0.1M Tris buffer at the tip, and backfilled with 3 M KCl. Using an intracellular amplifier (Neuroprobe Amplifier model 1600; A-M Systems, Carlsborg, WA), a single RGC was firstly filled with Lucifer Yellow with a few seconds of negative current, and then a continued positive current (0.6-1 nA) for 5 minutes for injecting Neurobiotin.

After microinjection, the whole-mount retinas were fixed in 4% paraformaldehyde (in 0.1

M PB) for 50-60 minutes, and then rinsed with 0.1 M PB six times for 10 min each. The injected cells were visualized by incubating the retinas with FITC-conjugated Streptavidin (diluted 1:50 in 0.1M PB with 0.1% Triton X-100; Vector Laboratories) at room temperature over night (or at least over eight hours) on a rotary shaker. After extensive wash for three hours in 0.1 M PB, the retinas were mounted ganglion cell side up in the mounting medium with DAPI (VectaShield, Vector Laboratories).

2.4 Light and electrical stimulations

Light stimuli generated by using Vision Work^{TM} 4.0 (Version 1.4.77; Vision Research Graphics, Durham) were displayed on a specialized microscopic mini-CRT monitor (refresh rate at 60 Hz; Lucivid, MicroBrightField, Colchester, VT). The ON or OFF RGCs were identified by their responses to a flash light spot of 200 μm diameter (500 ms) located on the soma center. The electrical stimulating device was a 2.45×2.45 mm^2 silicone-based subretinal chip obtained from the lab of Prof. CY Wu, National Chiao Tung University. A 532 nm laser (LIGHTLAS 532; LIGHTMED) was used to activate the solar cells on the chip to provide electrical currents.

To characterize the light responses of RGCs before electrical stimulation, two experimental paradigms were used. For determining the effect of light intensity on RGC responses, a flash light spot of 200 μm diameter (500 ms) was varied in different intensities (0, 1.1, 2.2, 3.3, 4.4, 5.6, 7.8, 8.9, and 10% of the maximum luminance that the mini-CRT monitor can produce). For

determining the effect of temporal frequency on RGC responses, a light flashing (34 ms) at 1, 2, 5, 10, and 20 Hz (occasionally 2.5 and 3.3 Hz were used) repeatedly for at least 10 times was applied. The inter-trial interval was 3 sec in these experiments.

To compare the responses of RGCs upon electrical stimulation with those of light stimulation, the same stimulus intensity effect and temporal frequency effect were examined after photoreceptors were bleached. For the stimulus intensity effect, a laser light pulse of 10 ms was varied at power values of 7, 9, 12, 18, 30, 60, 120, 300 mW. For the temporal frequency effect, the same 10 ms laser light pulse was applied repeatedly at 1, 2, 5, 10, and 20 Hz (occasionally 2.5 and 3.3 Hz were used) for at least 10 times. Similarly, the inter-trial interval was 3 sec in these experiments.

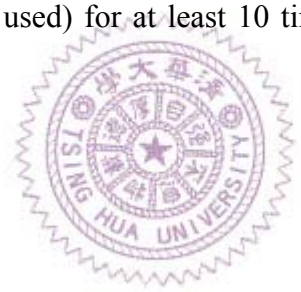

2.5 Extracellular recording

Retinal ganglion cells were recognized by DAPI staining under a 40× water immersion objective lens (Achroplan, NA 0.8, Zeiss). The responses of a single RGC were recorded by the loose-patch method (Hamill et al., 1981) with a borosilicate glass electrode (the impedance range 4-7 MΩ). The electrode was filled with filtered normal HEPES buffer (Nunemaker et al., 2003). Extracellular signals were amplified by a differential amplifier (ISO-80; National Instruments, Austin, TX). The responses of action potentials were recorded by a custom-written LabVIEW and the extracellular recording data were analyzed off-line by MATLAB (The MathWorks Inc;

Natick, MA).

2.6 Image acquisition

The injected cells were examined using a confocal scanning module (LSM 510; Carl Zeiss Meditec, Dublin, CA) on a flurescence microscope (Axioskop 2 Plus Mot; Carl Zeiss Meditec) with 20× (Plan-Neofluar, NA 0.5; Carl Zeiss Meditec) or 40× objective lens (Plan-Neofluar, NA 0.75; Carl Zeiss Meditec) at resolutions of 1024×1024. Z-stacks were acquired from the ganglion cell axon terminals to the level of the INL. The image overlaps were at least one half depth of each z plane. LSM 5 Image Examiner (v3.1.0.99, Zeiss) was used to adjust image intensity and contrast.

2.7 RGC tracing and classification

The general criteria of RGC classification were similar to those of Sun et al. (Sun et al., 2002). The morphological parameters used were (1) the diameter of dendritic field (estimated by assuming a circular shape of the dendritic area determined by convex polygon tracing), (2) the diameter of soma (estimated by assuming a circular shape of the soma area), (3) the dendritic stratification, obtained from the DAPI-labeled somata of confocal z series, (4) the dendritic arbor shape (Huxlin & Goodchild, 1997; Sun *et al.*, 2002). These parameters were measured using the LSM 5 Image Examiner.

4-8 cells from each type of RGCs were manually traced by Neurolucida analysis software (Neurolusida version 9; MicroBrightField, Williston, VT) with whole z-stack confocal image data. The Neurolucida tracing data were analyzed using the NeuroExplorer. Additional parameters were considered from NeuroExplorer analyses: total dendritic length, total number of dendritic branching points, and dendritic field area.

2.8 Data analysis

To calculate the cell density in the GCL, a square of 100×100 μm was centered at each confocal image, and all DAPI-labeled cells were counted manually. Total of 72, 25, 34, and 24 images from Group 1 RCS rats, Group 2 RCS rats, SD rats, and LE rats, respectively, were used and the average cell density was computed. To compare the difference among different groups, one-way ANOVA and *post hoc* Tukey's test were applied using the statistical program SPSS (version 17.0, IBM, NY).

CHAPTER 3

RESULTS

3.1 Morphological classification of RGCs in dystrophic RCS rats and normal rats

RGCs from two groups of dystrophic RCS rats (Group 1: P331-418; Group 2: P526-575) and two strains of normal rats (SD and LE) were classified according to the criteria (soma size, dendritic field size, dendritic stratification in the IPL, and number of primary dendrites) described in Sun et al. (2002). Although there were 7 types of RGCs with relatively large somata (20-25 μm in diameter) identified in this study (Table 1), only two types have sufficient numbers for cross-group comparison. They are A1 and A2 types of RGCs, and the A2 type can be further divided to inner and outer subtypes based on their dendritic stratifications in inner and outer layers of the IPL, respectively (Table 2). Other RGC types that were classified but did not have sufficient numbers for comparison were shown in Supplementary Materials (Table S1 and Fig. S1).

Figure 1 showed confocal images and Neurolucida tracings of A1 type of RG_A cells in four animal groups, which had polygonal somata and radiated branching patterns with Y-shaped dendrites that overlapped infrequently (Huxlin & Goodchild, 1997; Sun *et al.*, 2002). Figure 2 and 3 showed confocal images and Neurolucida tracings of A2 outer and inner types of RG_A cells in four animal groups which had round somata and repeated branching dentrites proximal to the cell body (Huxlin & Goodchild, 1997; Sun *et al.*, 2002).

3.2 Dendritic features of RGCs in dystrophic RCS rats and normal rats

It was suggested that level of stratification, extent of dendritic field, and density of branching are three major parameters for RGC classification (Kong et al., 2005). After using the level of stratification and extent of dendritic field for cell type classification, the dendritic field area, total dendritic length, and number of branching points obtained from Neurolucida tracings were further analyzed to compare dendritic features of RGCs in four animal groups (Fig. 4). These three parameters are the key characteristics of dendritic arborization, an indication of functional organization of synaptic inputs.

In the dendritic field area, all RG_A subtype cells of four animal groups did not have statistically significant difference (Fig. 4A-4C, left). In the total dendritic length, A1 cells from both groups of the RCS rats were significantly different from those from LE rats (Fig. 4A, center; the *p*-value of the ANOVA is 0.006; $p = 0.034$ for Group 1 vs. LE; $p = 0.016$ for Group 2 vs. LE from Tukey's test). For A2 outer cells, Group 1 and normal rats were also significantly different in the total dendritic length (Fig. 4B, center; the *p*-value of the ANOVA is 0.007; $p = 0.028$ for Group 1 vs. SD; $p = 0.018$ for Group 1 vs. LE from Tukey's test). For A2 inner cells, all four animal groups did not have statistically significant difference (Fig. 4C, center). In the number of branching points, A1 cells from all four animal groups did not have statistically significant difference (Fig. 4A, right). For A2 outer cells, both groups of the RCS rats were significantly different from the LE rats (Fig. 4B, right; the *p*-value of the ANOVA is 0.006; $p = 0.004$ for

Group 1 vs. LE; $p = 0.022$ for Group 2 vs. LE from Tukey's test). For A2 inner cells, all four animal groups did not have statistically significant difference (Fig. 4C, right). These results suggest that morphological features of RGCs in the RCS rats at later stages of degeneration differ from those of their normal control rats.

3.3 Tracer coupling pattern and dendritic beads of RGCs in dystrophic RCS rats and normal rats

Figure 5A showed confocal images of Neurobiotin injected RGCs from four animal groups. The tracer coupling patterns can be seen in three animal groups (Group 2 of RCS rats, SD and LE rats) except for Group 1 of RCS rats. By distinguishing RGCs with tracer coupling from non-coupling patterns, we showed that normal rats had significantly more tracer coupling cells than both groups of RCS rats (Fig. 5B; p-values were < 0.001 for two groups of RCS rats vs. normal rats; $p = 0.03$ for SD vs. LE from Chi-Square Test). It was noticeable that RGCs of RCS rats tend to have beads (bulges along dendritic segments) on their dendrites. Figure 5C showed examples of these dendritic beads for four animal groups. By distinguishing RGCs with dendritic beads from those without beads, we showed that both groups of RCS rats had significantly more cells with dendritic beads than normal rats (Fig. 5D; p-values were < 0.001 for two groups of RCS rats vs. normal rats; $p = 0.02$ for SD vs. LE from Chi-Square Test). These results suggest that the RCS rats at their later stages of degeneration exhibited abnormal communication with

neighboring cells and distorted dendritic integrity.

3.4 Cell number in the GCL and the IPL width in dystrophic RCS rats and normal rats

To examine if cell numbers in the GCL would decrease at late stages of degeneration in RCS rats, the DAPI positive cells in the GCL which includes ganglion cells and some amacrine cells were shown for all four groups of animals (Fig. 6A). By counting all DAPI positive cells in the GCL, we found that the cell numbers in Group 1 of RCS rats and in SD rats were significantly different (Fig. 6B; the *p*-value of the ANOVA is 0.025; $p = 0.015$ for Group 1 vs. SD from Tukey's test). To further examine if the IPL width would alter during retinal remodeling in RCS rats, the IPL widths from all four animal groups were compared. We found that the IPL widths of both groups of RCS rats were significantly different from those of normal control rats (Fig. 6C; the *p*-value of the ANOVA is < 0.001; $p = 0.003$ for Group 1 vs. Group 2; $p < 0.001$ for Group 1 vs. SD; $p = 0.001$ for Group 1 vs. LE; $p < 0.001$ for Group 2 vs. SD; $p < 0.001$ for SD vs. LE from Tukey's test). These results suggest that the RCS rats at their later stages of degeneration showed less viable cells in the GCL, and the retinal remodeling could result a loss of synaptic connections, thus thinning the width of the IPL.

3.5 Responses of RGCs upon light and electrical stimulations in normal rats

To compare responses of RGCs to electrical stimulation with those to normal light

stimulation, the same RGC was subjected to visual stimulation first, then electrical stimulation after bleaching photoreceptors (Fig. 7A). The normal SD rats were used to characterize RGC responses upon both light and electrical stimulations with a silicon-based subretinal array (Fig. 7B). An example of an ON RGC injected with Neurobiotin after recording revealed its dendritic morphology (Fig. 8A). In the light stimulated response, the average first spike latency for this cell appeared to decrease as the stimulus intensity increased (Fig. 8B), and the firing rate was increased when the stimulus was strengthened (Fig. 8C). This is consistent with previous results in studying rat RGCs (Cicerone & Green, 1980). Moreover, using a repetitive light stimulation, we found that the RGC responses were suppressed upon 1 Hz stimulation, and higher temporal frequencies suppressed the RGC responses even further (Fig. 8D). In the electrically stimulated response, the trend was apparently opposite, in that the RGC showed increased first spike latency as the laser power increased, except in the case of 1 Hz stimulation (Fig. 8E; the *p*-value of the ANOVA is 0.009; $p = 0.007$ for 70 mW vs. 200 mW of 2 Hz stimulation from Tukey's test), and the firing rate did not increase when the stimulus intensity strengthened, except in the case of 2 Hz stimulation (Fig. 8F; the *p*-value of the ANOVA is < 0.001; $p = 0.001$ for 70 mW vs. 100 mW in 2Hz; $p < 0.001$ for 70 mW vs. 200 mW of 2 Hz stimulation from Tukey's test). Upon repetitive electrical stimulation, the RGC seemed to show less suppression when the laser power was higher of 2 Hz stimulation (Fig. 2G). These results suggest that responses of RGCs upon light and electrical stimulations were different.

Unfortunately, the light stimulated responses of RGCs after light bleaching in other experiments can be found upon the strong laser stimulation (about 30 mW stimulus power, 5.6 nA current; data not show) even without having the chip underneath. Although the cause of this failure was not known, this makes the comparison between responses of RGCs upon light and electrical stimulations unreliable.

3.6 Responses of RGCs upon electrical stimulation in RCS rats

Despite the aforementioned unsuccessful study with normal rats, we decided to probe the physiology of RGCs upon electrical stimulation using RCS rats at their later stages of degeneration. As an example, a RGC of the P310 RCS rat retina was examined by using a 532 nm laser to evoke electrical current to stimulate the retina from the bipolar cell side. Various laser powers (7, 9, 12, 18, 30, 60, 120, and 300 mW) were applied in this experiment, but no distinguishable RGC responses were detected after the laser onset (Fig. 9). Moreover, RGC responses did not have statistically significant difference upon electrical stimulation by various laser powers (Fig. 9, bottom right). Based on these results, we conclude that this solar-cell based subretinal chip which activated by a 532 nm laser apparently cannot elicit RGC responses from the RCS rat at later degeneration stage.

CHAPTER 4

DISCUSSION

4.1 Changes of the RGC morphology in the RCS rat at the later degeneration stages

In the present study, we found that the dendritic features of RGCs in dystrophic RCS rats were significantly different from those of normal SD or LE rats in A1 and A2 outer RGC types (Fig. 4A&4B), and the A2 inner RGC type also showed moderate morphological changes in dystrophic RCS rats, although no statistically significant difference from normal rats was found (Fig. 4C). At these later stages of degeneration, the dendritic field area of RGCs in RCS rats was equivalent to that of normal rats, but the total dendritic length and number of branching points were significantly decreased. These observed changes might be explained by the retinal remodeling at phase 3 degeneration (Marc *et al.*, 2003; Jones & Marc, 2005). However, the study of RGC morphology in rd10 mice showed no changes of dendritic properties at 9 months of age (Mazzoni et al., 2008). The discrepancy between their study and our finding might arise from the different mechanism causing photoreceptor degeneration or the onset time of retinal remodeling. The RCS rat clearly lacks any visual inputs at P270 (Jones & Marc, 2005), but the aberrant cones persist up to at least 9 months in rd10 mice (Gargini et al., 2007).

It has been shown that number of RGCs in patients with RP was significantly lower than those in the control group (Stone *et al.*, 1992; Santos *et al.*, 1997), and this reduction of RGC number was age dependent (Gao & Hollyfield, 1992). In this study, change of cell number in the

GCL and the IPL width were also found in dystrophic RCS rats (Fig. 8). Previous studies using retrograde transport to examine the number of RGCs found no significant difference between control (RCS-dry^{+}) rats of P180 (Pavlidis et al., 2000) or of P153-515 (Eisenfeld et al., 1984) and RCS rats, but showed significantly different RGC number in RCS rats compared with SD rats (Sposato et al., 2008). Other studies indicate that the RGC axons were pulled into the inner retina in the RCS rat at 6 months of age or older, which is always associated with blood vessels (Villegas-Perez et al., 1998; Wang et al., 2005a). The serious cell migration might explain the IPL width change found in the present study (Fig. 6C), although the different strains of rats (RCS, SD and LE rats) might also influence the retinal thickness.

4.2 Abnormal communication of RGCs in the RCS rats

Most studies of RGC functions in the RCS rat were using electrophysiology or axon transport to investigate the relationships between RGCs and their presynaptic neurons or between RGCs and their centrally targeted neurons. In the present study, we showed the difference of tracer coupling pattern of RGCs in dystrophic RCS rats and normal rats, which suggests an abnormal communication of RGCs with neighboring RGCs and amacrine cells via gap junctions. Our findings that the tracer coupling patterns and dendritic beads in RCS rats were different from those of normal rats are consistent with the results found in diabetes and arterial hypertension patients (Meyer-Rusenberg et al., 2007). These abnormal characteristics might

explain the measured RGC electrophysiological properties (Chen et al., 2005) and the dendritic transport attenuation (Pavlidis et al., 2000).

4.3 Responses of RGCs upon electrical stimulation in normal rats

One major concern about the RGC responses upon electrical stimulation in normal rats is the failure of completely bleaching photoreceptors. In earlier experiments, retinal bleaching was conducted via continuous exposure of microscope's mercury-lamp light for 1 min or normal room light for 15 min. Although no RGC response upon the maximum light stimulation of the mini-CRT monitor was found after this bleaching protocol, the RGC responses upon the 532 nm laser stimulation can still be obtained. However, these RGC responses were not induced by the expected electrical stimulation (evoked by activating the multiphotodiode array via the 532 nm laser), because the RGC responded normally even without the subretinal chip placed under the retina. To improve the bleaching protocol, we have attempted to dissect the retina in room light condition for at least 2 hours (i.e., no dark adaption), or continuously expose the retina under the light-emitting diode (LED) flashlight for 15 min. However, both protocols failed to eliminate the RGC responses to the laser stimulation. Although continuous exposure of the retina under microscope's mercury-lamp light for 2 min could eliminate the RGCs responses to the laser stimulation, the spontaneous response of RGCs also disappeared. Under this bleaching protocol, the RGC responses upon electrical stimulation evoked by the maximum laser power (1500 mW,

about 1.03 mA current) were not found. However, by applying 50 mM KCl after this bleaching protocol, no sign of any RGC activity was found either. This suggests that this bleaching protocol was perhaps harmful to RGCs. Future experiments should seek the ambiguous laser source (eg., 810 nm infrared laser) to avoid activating two cone types in rats, which have the sensitivity peaks around 359 and 509 nm (Jacobs et al., 2001).

4.4 Responses of RGCs upon electrical stimulation in the RCS rats

In consistent with other RD animal studies (Zrenner *et al.*, 1999; Pu *et al.*, 2006; Stasheff, 2008; Sekirnjak *et al.*, 2009), we also found increased spontaneous activity in RGCs of the RCS rat (data not shown). In rd mice, the spontaneous oscillatory spike activity of RGCs can be decreased upon CNQX application, indicating the presynaptic origin (Petit-Jacques et al., 2005). In RCS rats, the microneuroma circuit (the bipolar, amacrine, and ganglion cells entwined processes at phase 3 of retinal remodeling) was modeled to suggest the oscillatory activity (Jones & Marc, 2005). However, cells with low spontaneous activity in the RCS rat were also recorded. Thus, the origin of changes of the RGC intrinsic properties in the RCS rat still remains to be determined (Marc et al., 2007; Margolis et al., 2008).

Upon electrical stimulation from the subretinal side, the RGC responses in the RCS rats were not found even applying the maximum laser power (1500 mW, about 1.03 mA current). In an experiment with patch-clamp recording of RGCs in the retinal slices of the RCS rat, the older

rats (9-12 weeks) showed diminishing action potential (Chen et al., 2005). In a study from Zrenner et al. (1999), the inhibition responses of RGCs upon subretinal electrical stimulation from a microelectrode array (MEA) in the RCS rat was observed. In another studies of subretinal stimulation in mammalian retinas, the current threshold for eliciting RGC responses was usually high (Jensen & Rizzo, 2006; 2007; 2008). It is possible that the laser spot (30 μm in diameter) used in the present study was too small to evoke enough electrical current for driving the RGC response. Alternatively, the retinal remodeling during the later stages of retinal degeneration may render the RGC unresponsive to low power of electrical stimulation.

4.5 Summary

Based on our results, the morphological features of RGCs in the inherited dystrophic RCS rat at their later stages of degeneration were significantly altered. This is consistent with the current hypothesis of retinal remodeling after photoreceptor degeneration (Jones and Marc, 2005), in that the neural structure and circuitry in RD models and RP patients are significantly affected. Thus, the present study implies that the strategy of treating patients with retinal degeneration needs to take into account of the increased spontaneous activities of RGCs and their altered morphological changes.

REFERENCES

Ames, A., 3rd & Nesbett, F.B. (1981) In vitro retina as an experimental model of the central nervous system. *J Neurochem*, **37**, 867-877.

Barhoum, R., Martinez-Navarrete, G., Corrochano, S., Germain, F., Fernandez-Sanchez, L., de la Rosa, E.J., de la Villa, P. & Cuenca, N. (2008) Functional and structural modifications during retinal degeneration in the rd10 mouse. *Neuroscience*, **155**, 698-713.

Bourne, M.C., Campbell, D.A. & Tansley, K. (1938) Hereditary Degeneration of the Rat Retina. *Br J Ophthalmol*, **22**, 613-623.

Chen, Z.S., Yin, Z.Q., Chen, S. & Wang, S.J. (2005) Electrophysiological changes of retinal ganglion cells in Royal College of Surgeons rats during retinal degeneration. *Neuroreport*, **16**, 971-975.

Chu, Y., Humphrey, M.F. & Constable, I.J. (1993) Horizontal cells of the normal and dystrophic rat retina: a wholemount study using immunolabelling for the 28-kDa calcium-binding protein. *Exp Eye Res*, **57**, 141-148.

Cicerone, C.M. & Green, D.G. (1980) Light adaptation within the receptive field centre of rat retinal ganglion cells. *J Physiol*, **301**, 517-534.

Cuenca, N., Pinilla, I., Sauve, Y. & Lund, R. (2005) Early changes in synaptic connectivity following progressive photoreceptor degeneration in RCS rats. *Eur J Neurosci*, **22**, 1057-1072.

D'Cruz, P.M., Yasumura, D., Weir, J., Matthes, M.T., Abderrahim, H., LaVail, M.M. & Vollrath, D. (2000) Mutation of the receptor tyrosine kinase gene Mertk in the retinal dystrophic RCS rat. *Hum Mol Genet*, **9**, 645-651.

de Jong, P.T. (2006) Age-related macular degeneration. *N Engl J Med*, **355**, 1474-1485.

DeVries, S.H. (2000) Bipolar cells use kainate and AMPA receptors to filter visual information into separate channels. *Neuron*, **28**, 847-856.

Dowling, J.E. & Sidman, R.L. (1962) Inherited retinal dystrophy in the rat. *J Cell Biol*, **14**, 73-109.

Eisenfeld, A.J., LaVail, M.M. & LaVail, J.H. (1984) Assessment of possible transneuronal changes in the retina of rats with inherited retinal dystrophy: cell size, number, synapses, and axonal transport by retinal ganglion cells. *J Comp Neurol*, **223**, 22-34.

Faktorovich, E.G., Steinberg, R.H., Yasumura, D., Matthes, M.T. & LaVail, M.M. (1990) Photoreceptor degeneration in inherited retinal dystrophy delayed by basic fibroblast growth factor. *Nature*, **347**, 83-86.

Fariss, R.N., Li, Z.Y. & Milam, A.H. (2000) Abnormalities in rod photoreceptors, amacrine cells, and horizontal cells in human retinas with retinitis pigmentosa. *Am J Ophthalmol*, **129**, 215-223.

Fried, S.I., Hsueh, H.A. & Werblin, F.S. (2006) A method for generating precise temporal patterns of retinal spiking using prosthetic stimulation. *J Neurophysiol*, **95**, 970-978.

Gal, A., Li, Y., Thompson, D.A., Weir, J., Orth, U., Jacobson, S.G., Apfelstedt-Sylla, E. & Vollrath, D. (2000) Mutations in MERTK, the human orthologue of the RCS rat retinal dystrophy gene, cause retinitis pigmentosa. *Nat Genet*, **26**, 270-271.

Gao, H. & Hollyfield, J.G. (1992) Aging of the human retina. Differential loss of neurons and retinal pigment epithelial cells. *Invest Ophthalmol Vis Sci*, **33**, 1-17.

Gargini, C., Terzibasi, E., Mazzoni, F. & Strettoi, E. (2007) Retinal organization in the retinal degeneration 10 (rd10) mutant mouse: a morphological and ERG study. *J Comp Neurol*, **500**, 222-238.

Hamel, C. (2006) Retinitis pigmentosa. *Orphanet J Rare Dis*, **1**, 40.

Hamill, O.P., Marty, A., Neher, E., Sakmann, B. & Sigworth, F.J. (1981) Improved patch-clamp techniques for high-resolution current recording from cells and cell-free membrane patches. *Pflugers Arch*, **391**, 85-100.

Hartong, D.T., Berson, E.L. & Dryja, T.P. (2006) Retinitis pigmentosa. *Lancet*, **368**, 1795-1809.

Huxlin, K.R. & Goodchild, A.K. (1997) Retinal ganglion cells in the albino rat: revised morphological classification. *J Comp Neurol*, **385**, 309-323.

Jacobs, G.H., Fenwick, J.A. & Williams, G.A. (2001) Cone-based vision of rats for ultraviolet and visible lights. *J Exp Biol*, **204**, 2439-2446.

Jager, R.D., Mieler, W.F. & Miller, J.W. (2008) Age-related macular degeneration. *N Engl J Med*, **358**, 2606-2617.

Jensen, R.J. & Rizzo, J.F., 3rd (2006) Thresholds for activation of rabbit retinal ganglion cells with a subretinal electrode. *Exp Eye Res*, **83**, 367-373.

Jensen, R.J. & Rizzo, J.F., 3rd (2007) Responses of ganglion cells to repetitive electrical stimulation of the retina. *J Neural Eng*, **4**, S1-6.

Jensen, R.J. & Rizzo, J.F., 3rd (2008) Activation of retinal ganglion cells in wild-type and rd1 mice through electrical stimulation of the retinal neural network. *Vision Res*, **48**, 1562-1568.

Jensen, R.J., Ziv, O.R. & Rizzo, J.F., 3rd (2005) Thresholds for activation of rabbit retinal ganglion cells with relatively large, extracellular microelectrodes. *Invest Ophthalmol Vis Sci*, **46**, 1486-1496.

Jones, B.W. & Marc, R.E. (2005) Retinal remodeling during retinal degeneration. *Exp Eye Res*, **81**, 123-137.

Kong, J.H., Fish, D.R., Rockhill, R.L. & Masland, R.H. (2005) Diversity of ganglion cells in the mouse retina: unsupervised morphological classification and its limits. *J Comp Neurol*, **489**, 293-310.

Lagali, P.S., Balya, D., Awatramani, G.B., Munch, T.A., Kim, D.S., Busskamp, V., Cepko, C.L. & Roska, B. (2008) Light-activated channels targeted to ON bipolar cells restore visual function in retinal degeneration. *Nat Neurosci*, **11**, 667-675.

LaVail, M.M. & Battelle, B.A. (1975) Influence of eye pigmentation and light deprivation on inherited retinal dystrophy in the rat. *Exp Eye Res*, **21**, 167-192.

LaVail, M.M., Sidman, R.L. & O'Neil, D. (1972) Photoreceptor-pigment epithelial cell relationships in rats with inherited retinal degeneration. Radioautographic and electron microscope evidence for a dual source of extra lamellar material. *J Cell Biol*, **53**, 185-209.

Lin, B., Koizumi, A., Tanaka, N., Panda, S. & Masland, R.H. (2008) Restoration of visual function in retinal degeneration mice by ectopic expression of melanopsin. *Proc Natl Acad Sci U S A*, **105**, 16009-16014.

Machida, S., Raz-Prag, D., Fariss, R.N., Sieving, P.A. & Bush, R.A. (2008) Photopic ERG negative response from amacrine cell signaling in RCS rat retinal degeneration. *Invest Ophthalmol Vis Sci*, **49**, 442-452.

MacLaren, R.E., Pearson, R.A., MacNeil, A., Douglas, R.H., Salt, T.E., Akimoto, M., Swaroop, A., Sowden, J.C. & Ali, R.R. (2006) Retinal repair by transplantation of photoreceptor precursors. *Nature*, **444**, 203-207.

Marc, R.E., Jones, B.W., Anderson, J.R., Kinard, K., Marshak, D.W., Wilson, J.H., Wensel, T. & Lucas, R.J. (2007) Neural reprogramming in retinal degeneration. *Invest Ophthalmol Vis Sci*, **48**, 3364-3371.

Marc, R.E., Jones, B.W., Watt, C.B. & Strettoi, E. (2003) Neural remodeling in retinal degeneration. *Prog Retin Eye Res*, **22**, 607-655.

Margolis, D.J., Newkirk, G., Euler, T. & Detwiler, P.B. (2008) Functional stability of retinal ganglion cells after degeneration-induced changes in synaptic input. *J Neurosci*, **28**, 6526-6536.

Masland, R.H. (2001) The fundamental plan of the retina. *Nat Neurosci*, **4**, 877-886.

Masu, M., Iwakabe, H., Tagawa, Y., Miyoshi, T., Yamashita, M., Fukuda, Y., Sasaki, H., Hiroi, K., Nakamura, Y., Shigemoto, R. & et al. (1995) Specific deficit of the ON response in visual transmission by targeted disruption of the mGluR6 gene. *Cell*, **80**, 757-765.

Mazzoni, F., Novelli, E. & Strettoi, E. (2008) Retinal ganglion cells survive and maintain normal

dendritic morphology in a mouse model of inherited photoreceptor degeneration. *J Neurosci*, **28**, 14282-14292.

Meyer-Rusenberg, B., Pavlidis, M., Stupp, T. & Thanos, S. (2007) Pathological changes in human retinal ganglion cells associated with diabetic and hypertensive retinopathy. *Graefes Arch Clin Exp Ophthalmol*, **245**, 1009-1018.

Mullen, R.J. & LaVail, M.M. (1976) Inherited retinal dystrophy: primary defect in pigment epithelium determined with experimental rat chimeras. *Science*, **192**, 799-801.

Nunemaker, C.S., DeFazio, R.A. & Moenter, S.M. (2003) A targeted extracellular approach for recording long-term firing patterns of excitable cells: a practical guide. *Biol Proced Online*, **5**, 53-62.

Pavlidis, M., Fischer, D. & Thanos, S. (2000) Photoreceptor degeneration in the RCS rat attenuates dendritic transport and axonal regeneration of ganglion cells. *Invest Ophthalmol Vis Sci*, **41**, 2318-2328.

Perry, J., Du, J., Kjeldbye, H. & Gouras, P. (1995) The effects of bFGF on RCS rat eyes. *Curr Eye Res*, **14**, 585-592.

Petit-Jacques, J., Volgyi, B., Rudy, B. & Bloomfield, S. (2005) Spontaneous oscillatory activity of starburst amacrine cells in the mouse retina. *J Neurophysiol*, **94**, 1770-1780.

Pu, M., Xu, L. & Zhang, H. (2006) Visual response properties of retinal ganglion cells in the royal college of surgeons dystrophic rat. *Invest Ophthalmol Vis Sci*, **47**, 3579-3585.

Ray, A., Sun, G.J., Chan, L., Grzywacz, N.M., Weiland, J. & Lee, E.J. (2010) Morphological alterations in retinal neurons in the S334ter-line3 transgenic rat. *Cell Tissue Res*, **339**, 481-491.

Santos, A., Humayun, M.S., de Juan, E., Jr., Greenburg, R.J., Marsh, M.J., Klock, I.B. & Milam, A.H. (1997) Preservation of the inner retina in retinitis pigmentosa. A morphometric analysis. *Arch Ophthalmol*, **115**, 511-515.

Sekirnjak, C., Hottowy, P., Sher, A., Dabrowski, W., Litke, A.M. & Chichilnisky, E.J. (2008)

High-resolution electrical stimulation of primate retina for epiretinal implant design. *J Neurosci*, **28**, 4446-4456.

Sekirnjak, C., Hulse, C., Jepson, L.H., Hottowy, P., Sher, A., Dabrowski, W., Litke, A.M. & Chichilnisky, E.J. (2009) Loss of responses to visual but not electrical stimulation in ganglion cells of rats with severe photoreceptor degeneration. *J Neurophysiol*, **102**, 3260-3269.

Shyu, J.S., Maia, M., Weiland, J.D., Ohearn, T., Chen, S.J., Margalit, E., Suzuki, S. & Humayun, M.S. (2006) Electrical stimulation in isolated rabbit retina. *IEEE Trans Neural Syst Rehabil Eng*, **14**, 290-298.

Sidman, R.L., Pearlstein, R. & Waymouth, C. (1965) Pink-eyed dilution (p) gene in rodents: increased pigmentation in tissue culture. *Dev Biol*, **12**, 93-116.

Sposato, V., Iovieno, A., Sornelli, F. & Aloe, L. (2008) Axonal transport deficit in the optic nerve of rats with inherited retinitis pigmentosa and experimentally induced glaucoma. *Graefes Arch Clin Exp Ophthalmol*, **246**, 1553-1558.

Stasheff, S.F. (2008) Emergence of sustained spontaneous hyperactivity and temporary preservation of OFF responses in ganglion cells of the retinal degeneration (rd1) mouse. *J Neurophysiol*, **99**, 1408-1421.

Stone, J.L., Barlow, W.E., Humayun, M.S., de Juan, E., Jr. & Milam, A.H. (1992) Morphometric analysis of macular photoreceptors and ganglion cells in retinas with retinitis pigmentosa. *Arch Ophthalmol*, **110**, 1634-1639.

Strauss, O. (2005) The retinal pigment epithelium in visual function. *Physiol Rev*, **85**, 845-881.

Sullivan, R.K., Woldemussie, E. & Pow, D.V. (2007) Dendritic and synaptic plasticity of neurons in the human age-related macular degeneration retina. *Invest Ophthalmol Vis Sci*, **48**, 2782-2791.

Sun, W., Li, N. & He, S. (2002) Large-scale morophological survey of rat retinal ganglion cells. *Vis Neurosci*, **19**, 483-493.

Thyagarajan, S., van Wyk, M., Lehmann, K., Lowel, S., Feng, G. & Wassle, H. (2010) Visual function in mice with photoreceptor degeneration and transgenic expression of channelrhodopsin 2 in ganglion cells. *J Neurosci*, **30**, 8745-8758.

Villegas-Perez, M.P., Lawrence, J.M., Vidal-Sanz, M., Lavail, M.M. & Lund, R.D. (1998) Ganglion cell loss in RCS rat retina: a result of compression of axons by contracting intraretinal vessels linked to the pigment epithelium. *J Comp Neurol*, **392**, 58-77.

Wang, S., Lu, B., Girman, S., Holmes, T., Bischoff, N. & Lund, R.D. (2008) Morphological and functional rescue in RCS rats after RPE cell line transplantation at a later stage of degeneration. *Invest Ophthalmol Vis Sci*, **49**, 416-421.

Wang, S., Lu, B. & Lund, R.D. (2005a) Morphological changes in the Royal College of Surgeons rat retina during photoreceptor degeneration and after cell-based therapy. *J Comp Neurol*, **491**, 400-417.

Wang, S., Lu, B., Wood, P. & Lund, R.D. (2005b) Grafting of ARPE-19 and Schwann cells to the subretinal space in RCS rats. *Invest Ophthalmol Vis Sci*, **46**, 2552-2560.

Wassle, H. (2004) Parallel processing in the mammalian retina. *Nat Rev Neurosci*, **5**, 747-757.

Wright, A.F., Chakarova, C.F., Abd El-Aziz, M.M. & Bhattacharya, S.S. (2010) Photoreceptor degeneration: genetic and mechanistic dissection of a complex trait. *Nat Rev Genet*, **11**, 273-284.

Zrenner, E. (2002) Will retinal implants restore vision? *Science*, **295**, 1022-1025.

Zrenner, E., Stett, A., Weiss, S., Aramant, R.B., Guenther, E., Kohler, K., Miliczek, K.D., Seiler, M.J. & Haemmerle, H. (1999) Can subretinal microphotodiodes successfully replace degenerated photoreceptors? *Vision Res*, **39**, 2555-2567.

TABLES

Table 1 Summary of RGC types classified and analyzed for different age groups of the dystrophic RCS rats and the normal rats (SD and LE)

	RCS rat				SD rat		LE rat	
	Group 1 (P331-418)		Group 2 (P526-575)		P54-85		P45-46	
RGC type	Classified	Analyzed	Classified	Analyzed	Classified	Analyzed	Classified	Analyzed
A1	16	8	11	8	12	5	6	6
A2 outer	10	6	9	6	7	5	4	4
A2 inner	30	8	19	6	15	5	11	5
B3 outer	1	0	0	0	0	0	0	0
C1	1	0	0	0	0	0	0	0
C2 outer	6	0	0	0	0	0	5	0
C2 inner	8	0	1	0	0	0	0	0
C3	7	0	3	0	1	0	0	0
C4 outer	0	0	2	0	0	0	0	0
C4 inner	1	0	0	0	0	0	0	0
Total	80	22	45	20	35	15	26	15
Number of retina	19	13	11	8	5	5	6	5

*Cell type classification was followed Sun et al. (2002), and morphological analysis was done using Neurolucida.

Table 2 Summary of quantitative data for different age groups of the dystrophic RCS rats and the normal rats (SD and LE)

RGC type		Classified cells				Analyzed cells		
		Soma diameter (μm)	**Dendritic field diameter (μm)**	**Stratification (% IPL depth)**	**No. of primary dendrites**	**Dendritic field area (μm^2)**	**Total dendritic length (μm)**	**No. of branching points**
A1	Group 1	21.2 ± 0.64	369.5 ± 24.62	84.7 ± 1.88	4 - 7	123,869.8 ± 26,592.94	3,991.2 ± 455.22	33.4 ± 4.07
	Group 2	25.0 ± 1.38	318.5 ± 24.53	82.1 ± 2.73	4 - 7	106,791.3 ± 20,880.33	3,627.7 ± 412.13	31.6 ± 4.39
	SD	25.5 ± 0.87	439.1 ± 24.20	74.3 ± 3.83	3 - 7	190,339.8 ± 25,594.29	6,384.4 ± 438.66	50.2 ± 7.77
	LE	21.7 ± 1.09	514.4 ± 44.02	72.9 ± 3.13	4 - 6	220,049.0 ± 36,806.27	6,666.5 ± 772.74	41.8 ± 6.23
A2 outer	Group 1	22.6 ± 0.82	315.8 ± 11.06	34.9 ± 3.76	4 - 9	106,042.5 ± 13,730.77	4,426.6 ± 136.66	43.8 ± 4.18
	Group 2	23.6 ± 1.53	308.8 ± 21.20	35.5 ± 3.85	5 - 7	126,869.9 ± 23,240.83	5,382.0 ± 533.49	54.8 ± 3.02
	SD	23.5 ± 1.36	354.1 ± 23.18	33.2 ± 2.76	4 - 7	137,700.6 ± 17,331.20	6,644.4 ± 338.36	60.2 ± 6.56
	LE	22.0 ± 1.39	371.2 ± 43.21	45.4 ± 3.76	4 - 7	142,665.7 ± 24,543.02	6,954.9 ± 867.79	80.0 ± 10.47
A2 inner	Group 1	22.1 ± 0.46	353.5 ± 13.65	74.2 ± 1.76	4 - 9	126,054.2 ± 16,083.12	4,892.8 ± 558.19	50.6 ± 7.10
	Group 2	23.5 ± 0.85	327.4 ± 12.40	71.6 ± 2.81	4 - 7	106,952.3 ± 14,173.41	4,740.1 ± 205.29	49.2 ± 7.13
	SD	26.0 ± 0.78	432.0 ± 13.86	66.1 ± 1.58	4 - 7	156,707.0 ± 20,963.09	6,450.1 ± 949.54	63.8 ± 16.09
	LE	23.0 ± 0.68	410.3 ± 28.18	69.1 ± 3.11	4 - 8	132,215.6 ± 20,822.40	7,106.6 ± 1,219.65	86.2 ± 13.86

*Cell type classification was followed Sun et al. (2002), and morphological analysis was done using Neurolucida.

**Each value represents Mean ± SE, except the No. of primary dendrites.

FIGURES

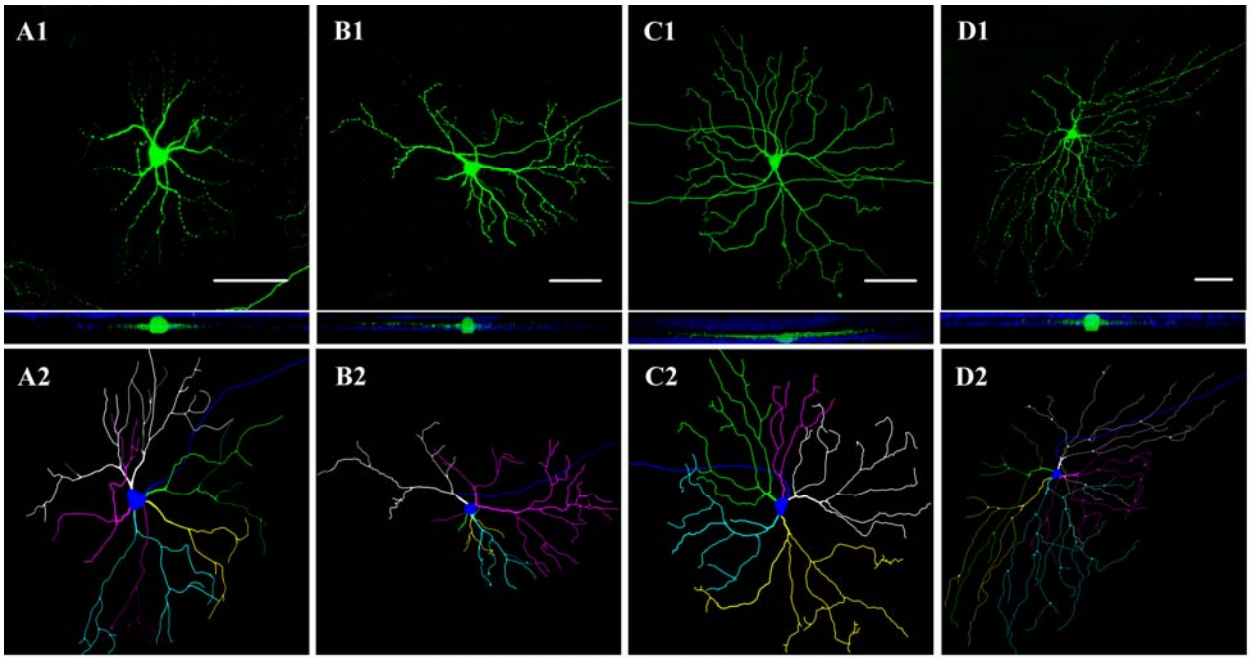

Figure 1 Dendritic morphologies of RG_{A1} cells in dystrophic RCS rats and normal rats. (A) Confocal image of the RGC of Group 1 RCS rats (A1) and the Neurolucida tracing (A2). (B) Confocal image of the RGC of Group 2 RCS rats (B1) and the Neurolucida tracing (B2). (C) Confocal image of the RGC of SD rats (C1) and the Neurolucida tracing (C2). (D) Confocal image of the RGC of LE rats (D1) and the Neurolucida tracing (D2). Green, Neurobiotin; blue, DAPI. Different colors in the Neurolucida tracing indicate different dendritic branches. Scale bar, 100 μm.

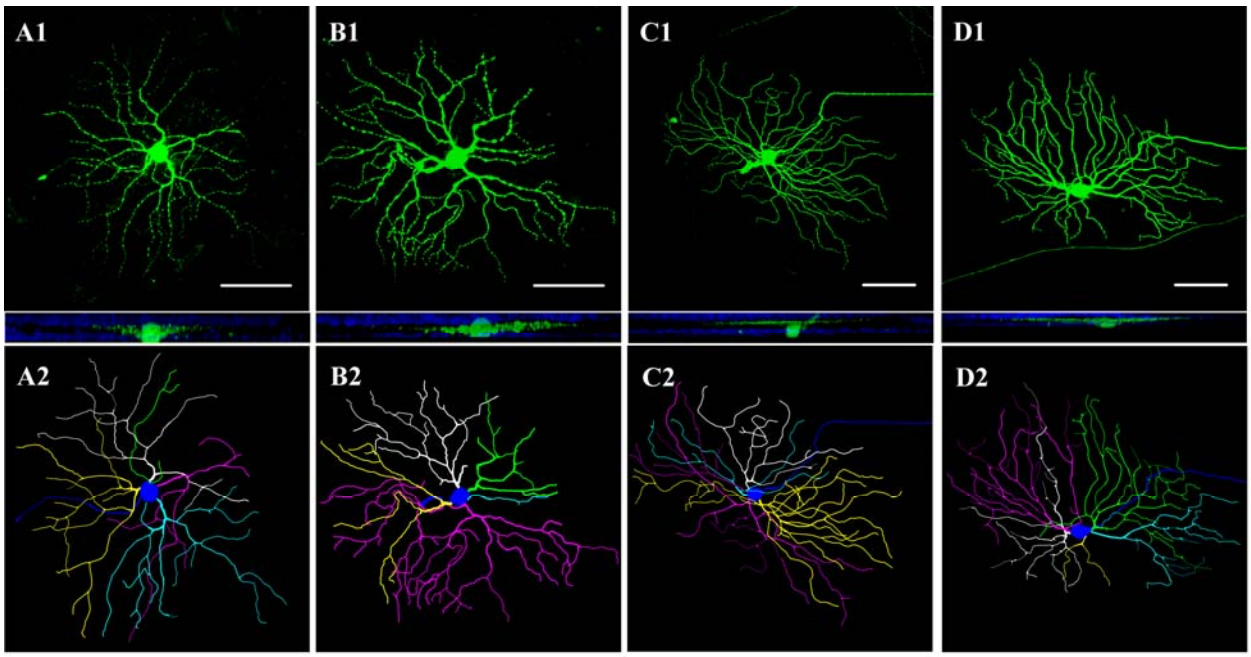

Figure 2 Dendritic morphologies of $RG_{A2\ outer}$ cells in dystrophic RCS rats and normal rats.

(A) Confocal image of the RGC of Group 1 RCS rats (A1) and the Neurolucida tracing (A2). (B) Confocal image of the RGC of group 2 RCS rats (B1) and the Neurolucida tracing (B2). (C) Confocal image of the RGC of SD rats (C1) and the Neurolucida tracing (C2). (D) Confocal image of the RGC of LE rats (D1) and the Neurolucida tracing (D2). Green, Neurobiotin; blue: DAPI. Different colors in the Neurolucida tracing indicate different dendritic branches. Scale bar, 100 μm.

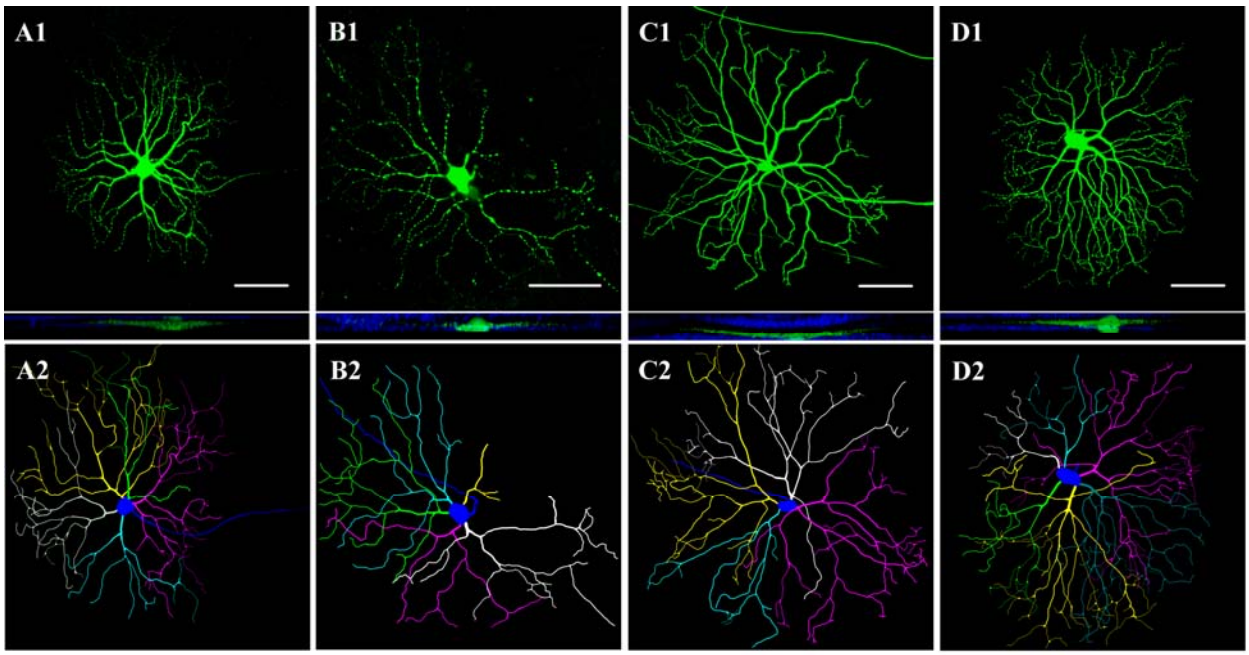

Figure 3 Dendritic morphologies of $RG_{A2\ inner}$ cells in dystrophic RCS rats and normal rats.

(A) Confocal image of the RGC of Group 1 RCS rats (A1) and the Neurolucida tracing (A2). (B) Confocal image of the RGC of group 2 RCS rats (B1) and the Neurolucida tracing (B2). (C) Confocal image of the RGC of SD rats (C1) and the Neurolucida tracing (C2). (D) Confocal image of the RGC of LE rats (D1) and the Neurolucida tracing (D2). Green, Neurobiotin; blue, DAPI. Different colors in the Neurolucida tracing indicate different dendritic branches. Scale bar, 100 μm.

.

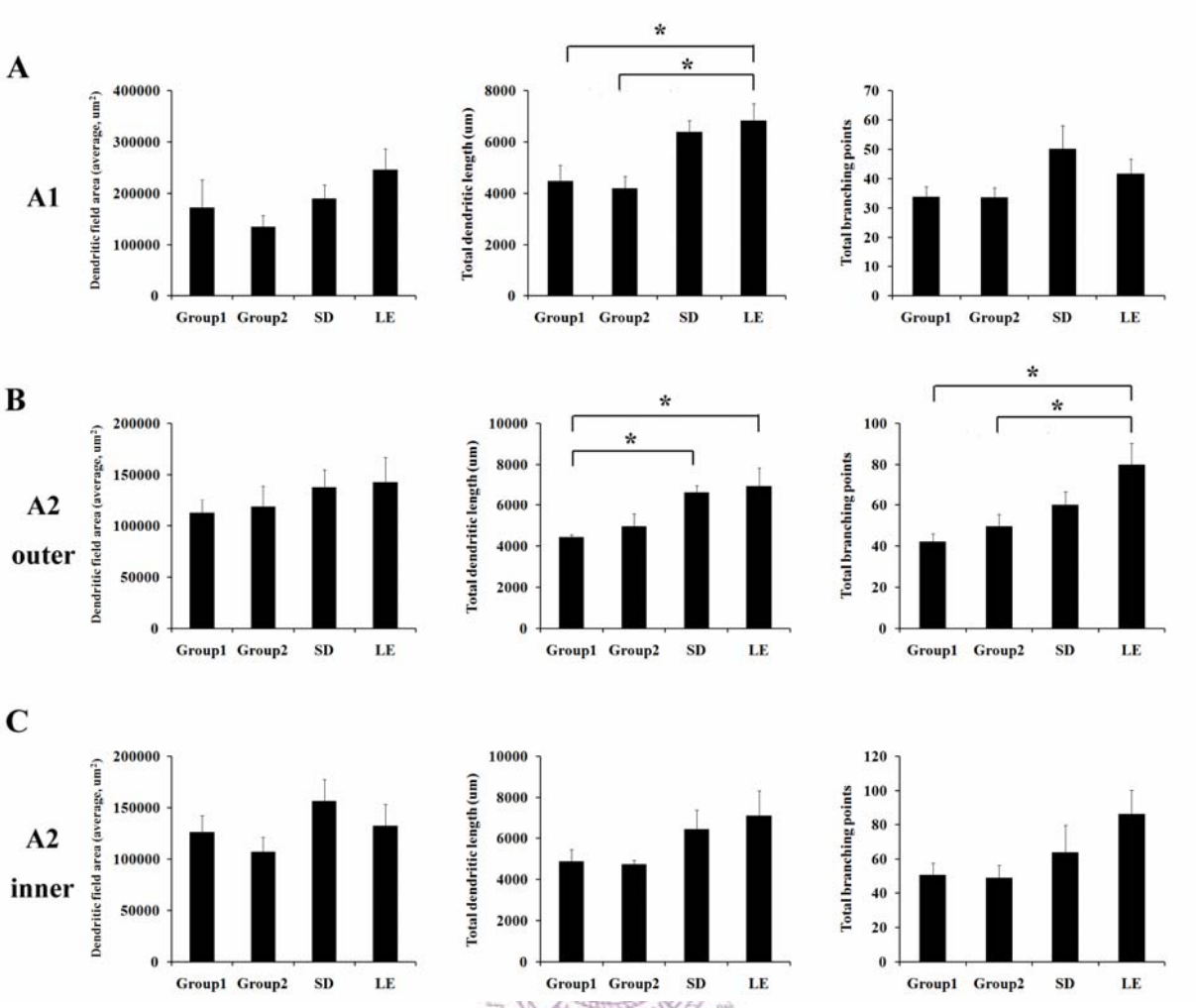

Figure 4 Morphological analyses of three types of RGCs in dystrophic RCS rats and normal rats. Three parameters (dendritic field area, total dendritic length, and total branching points) obtained from Neurolucida tracings were compared among different groups of rats. (A) A1 type RGCs. (B) A2 outer type RGCs. (C) A2 inner type RGCs. Error bar indicates Mean ± SE. Asteroid indicates statistical significance for p-value < 0.05.

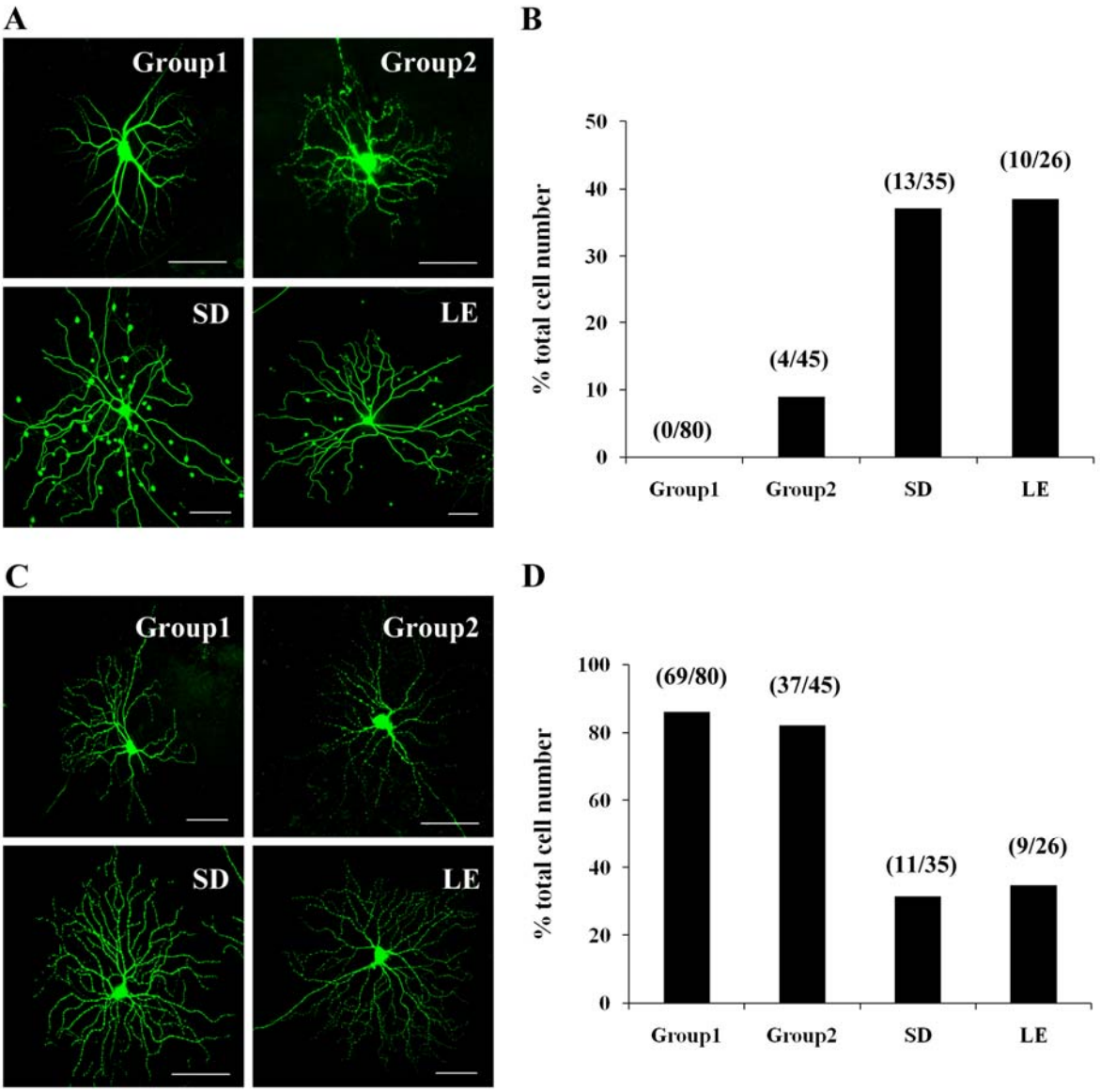

Figure 5 Tracer coupling patterns and dendritic beads of RGCs in dystrophic RCS rats and normal rats. (A) Confocal images of A1, A2, A1, and A1 types of RGCs in Group 1 RCS, Group 2 RCS, SD, and LE rats, respectively. Tracer coupling patterns can be seen in Group 2 RCS, SD, and LE rats. (B) Percentage of coupled cells in four groups of rats. Brackets show RGCs with coupled cells and total RGCs (C) Confocal images of A2, A2, A2, and A2 types of RGCs in Group 1 RCS, Group 2 RCS, SD, and LE rats, respectively. Dendritic beads can be seen

easily in Groups 1 and 2 RCS rats. (D) Percentage of cells with dendritic beads in four groups of rats. Brackets show RGCs with dendritic beads and total RGCs. Scale bar, 100 μm.

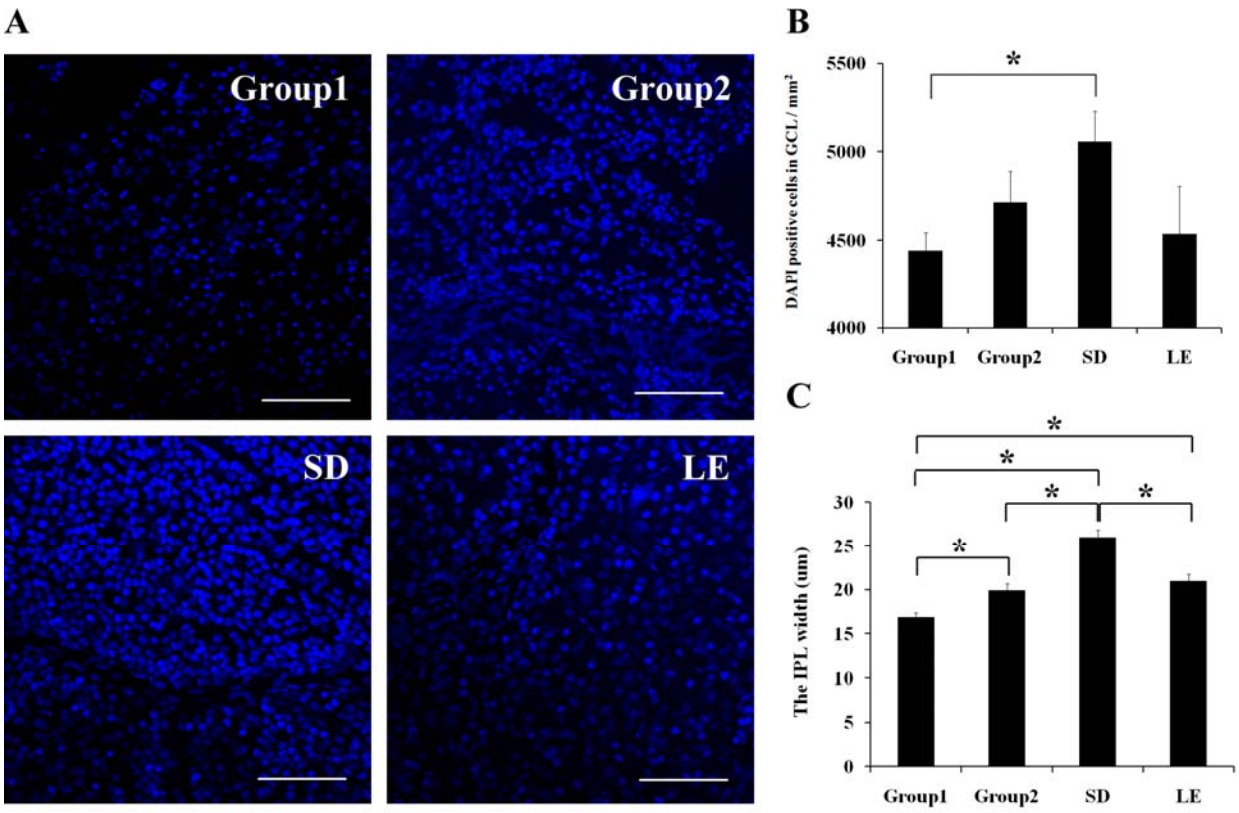

Figure 6 DAPI positive cells in the GCL and the IPL width in dystrophic RCS rats and normal rats. (A) Confocal images of DAPI positive cells in GCL for Groups 1 and 2 RCS rats, SD, and LE rats. (B) Average number of DAPI positive cells in the GCL in Group 1 RCS rats (n=72), Group 2 RCS rats (n=25), SD rats (n=34), and LE rats (n=24). (C) Average IPL width in Group 1 RCS rats (n=80), Group 2 RCS rats (n=45), SD rats (n=35), and LE rats (n=26). Scale bar, 100 μm. Cell numbers are indicated in parentheses. Error bar indicates Mean ± SE. Asteroid indicates statistical significance for *p*-value < 0.05.

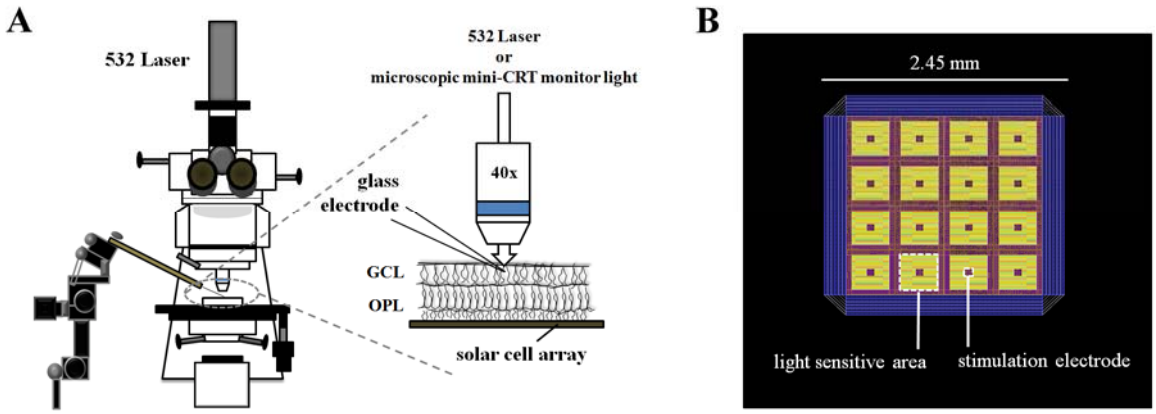

Figure 7 Schematic diagram of experimental design and the retinal chip. (A) The 532 laser or visual stimulus (from a microscopic mini-CRT monitor) positioned on the top of the microscope was used to project light onto the retinal chip. The responses of RGCs were recorded using a loose-patch electrode. A piece of the isolated rat retina was attached to the silicone-based subretinal photodiode array with its ganglion cell side up. (B) The solar cell subretinal chip is 2.45×2.45 mm^2 with 4×4 pixels (light sensitive area). The stimulation electrode (75×75 μm) is at the center of each pixel (490×490 μm), and the returning ground is the surrounding of each pixel. GCL, ganglion cell layer; OPL, outer plexiform layer.

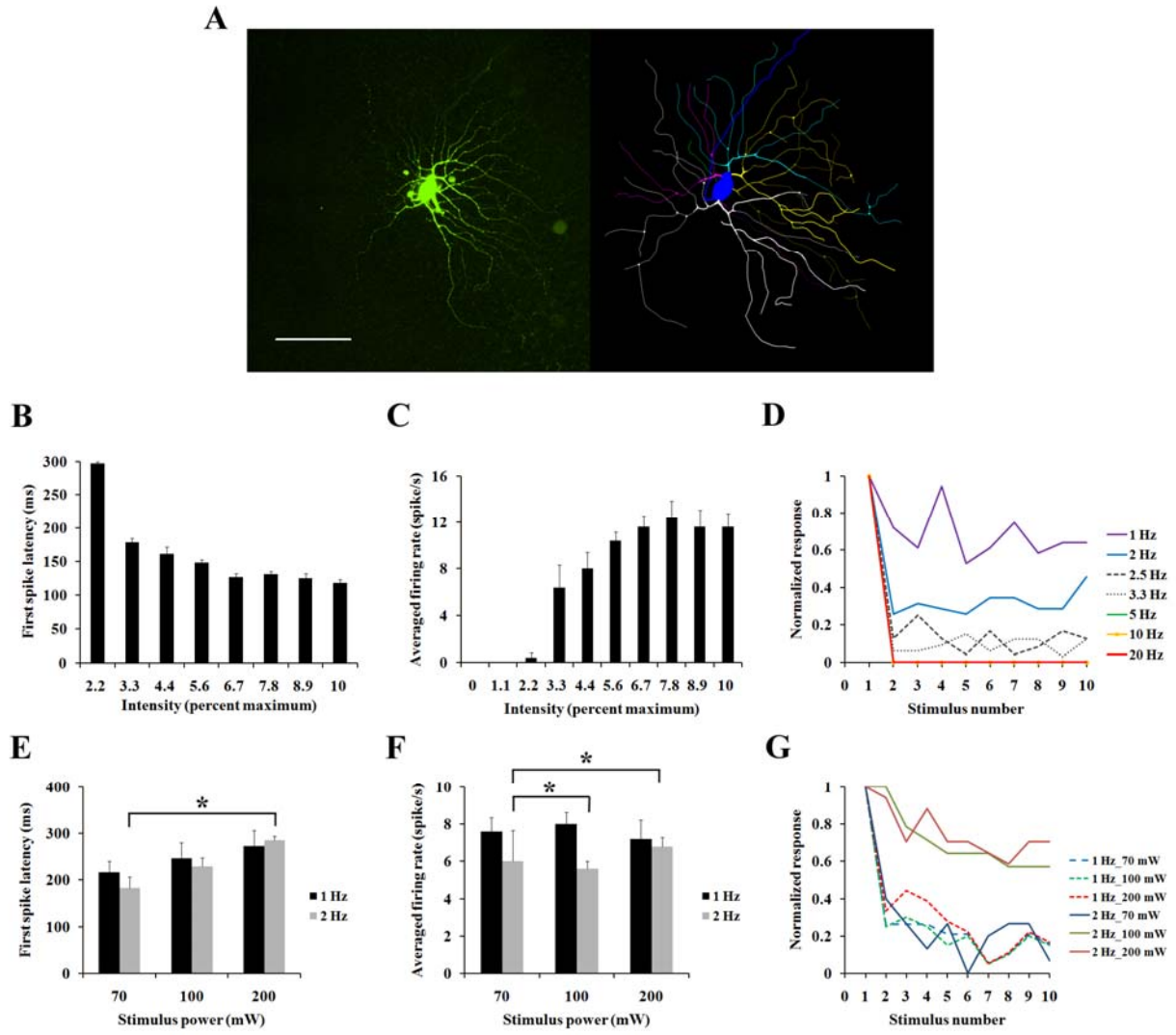

Figure 8 Responses of an ON RGC upon light and electrical stimulations in a normal P145 SD rat. (A) Dendritic morphology of a recorded ON RGC. (Left) Confocal image; (Right) Drawing of Neurolucida. Different colors indicate different dentritic branchings. Scale bar, 100 μm. (B) First spike latency of the RGC under different light intensities. The light intensity was normalized to the maximum luminance of the microscopic mini-CRT monitor. (C) Averaged firing rate of the RGC under different light intensities. (D) Normalized responses of the RGC upon 10 repetitive visual stimulations at different temporal frequencies. The light intensity was the maximum luminance of the monitor. All responses were normalized to the first stimulation

for each frequency. (E) First spike latency of the RGC under three different strengths of electrical stimulation at two different temporal frequencies. (F) Averaged firing rate of the RGC under three different strengths of electrical stimulation at two different temporal frequencies. (G) Normalized responses of the RGC upon 10 repetitive electrical stimulations at different strengths and temporal frequencies. All responses were normalized to the first stimulation for each frequency and strength. Error bar indicates Mean ± SE. Asteroid indicates statistical significance for p-value < 0.05.

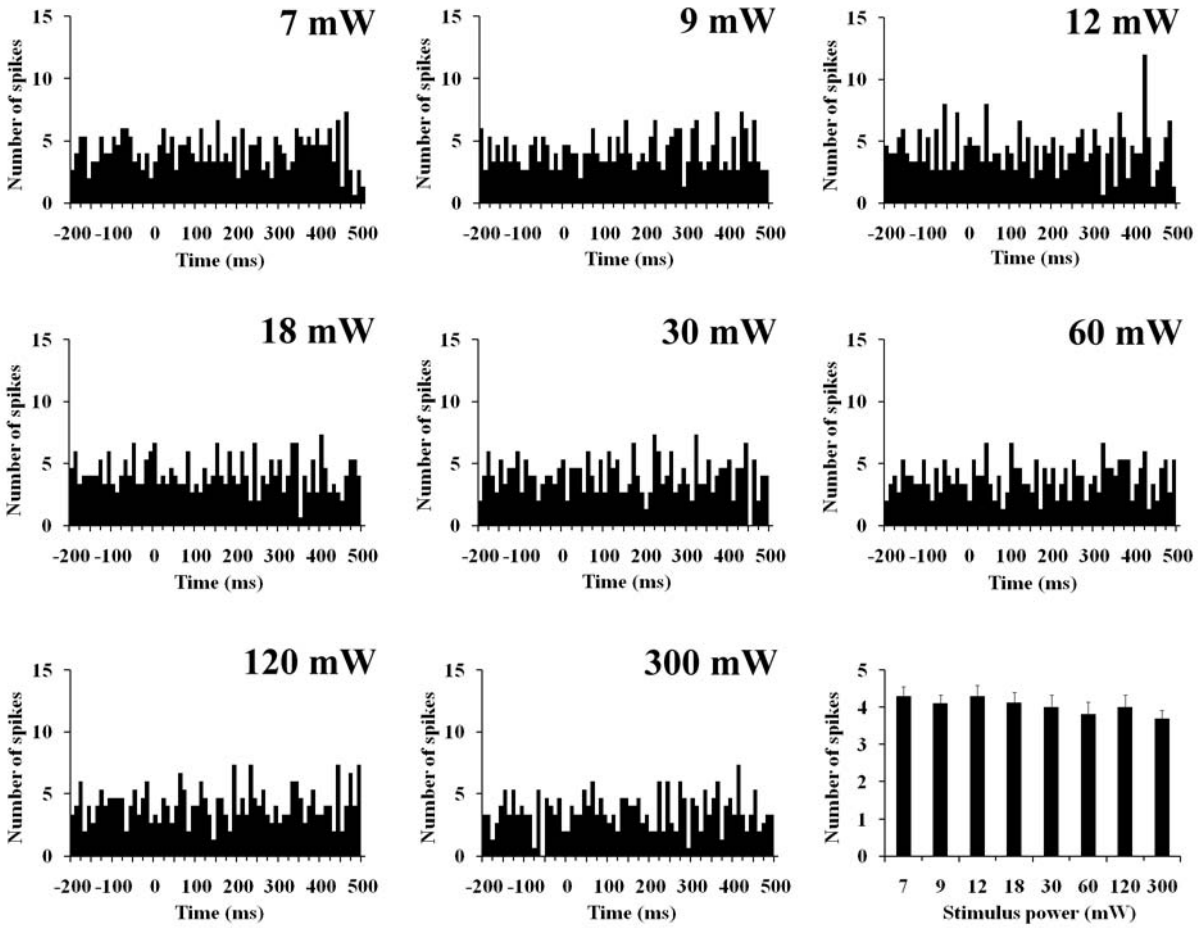

Figure 9 Responses of an RGC to electrical stimulations of 8 different laser powers in a P310 RCS rat. Histograms were averaged for 3 repeated trials, and solar-cell based chip stimulation onset was at time 0 ms. The bin size was 10 ms. Bottom right panel is the average RGC responses after electrical stimulation for 200 ms. Error bar indicates Mean ± SE.

SUPPLEMENTARY MATERIALS

Table S1. Summary of quantitative data of other RGC types in the different age groups of the dystrophic RCS rats and the normal rats (SD and LE)

RGC type		Soma diameter (μm)	DF diameter (μm)	Stratification (% IPL depth)	No. of Primary dendrites
B3 outer	Group 1	21.1	285.0	45.2	5
	Group 2	N/A	N/A	N/A	N/A
	SD	N/A	N/A	N/A	N/A
	LE	N/A	N/A	N/A	N/A
C1	Group 1	17.5	246.0	76.6	4
	Group 2	N/A	N/A	N/A	N/A
	SD	N/A	N/A	N/A	N/A
	LE	N/A	N/A	N/A	N/A
C2 outer	Group 1	19.8 ± 1.16	285.2 ± 37.87	36.9 ± 3.67	4 - 8
	Group 2	N/A	N/A	N/A	N/A
	SD	N/A	N/A	N/A	N/A
	LE	N/A	N/A	N/A	N/A
C2 inner	Group 1	19.1 ± 0.75	288.7 ± 26.84	69.0 ± 3.86	4 - 6
	Group 2	21.9	345.1	75.0	7
	SD	N/A	N/A	N/A	N/A
	LE	23.1 ± 1.08	240.4 ± 12.55	65.6 ± 4.60	5 - 6
C3	Group 1	18.0 ± 1.42	366.3 ± 19.10	73.7 ± 3.74	4 - 8
	Group 2	24.2 ± 1.16	325.9 ± 68.64	63.4 ± 8.53	5 - 7
	SD	18.2	411.7	62.6	6
	LE	N/A	N/A	N/A	N/A
C4 outer	Group 1	24.3	228.1	65.9	5
	Group 2	N/A	N/A	N/A	N/A
	SD	N/A	N/A	N/A	N/A
	LE	N/A	N/A	N/A	N/A
C4 inner	Group 1	N/A	N/A	N/A	N/A
	Group 2	18.0 ± 1.80	213.8 ± 17.03	40.3 ± 4.98	4 - 5
	SD	N/A	N/A	N/A	N/A
	LE	N/A	N/A	N/A	N/A

*Each value represents Mean ± SE or Mean (when n=1), except for the No. of primary dendrites.

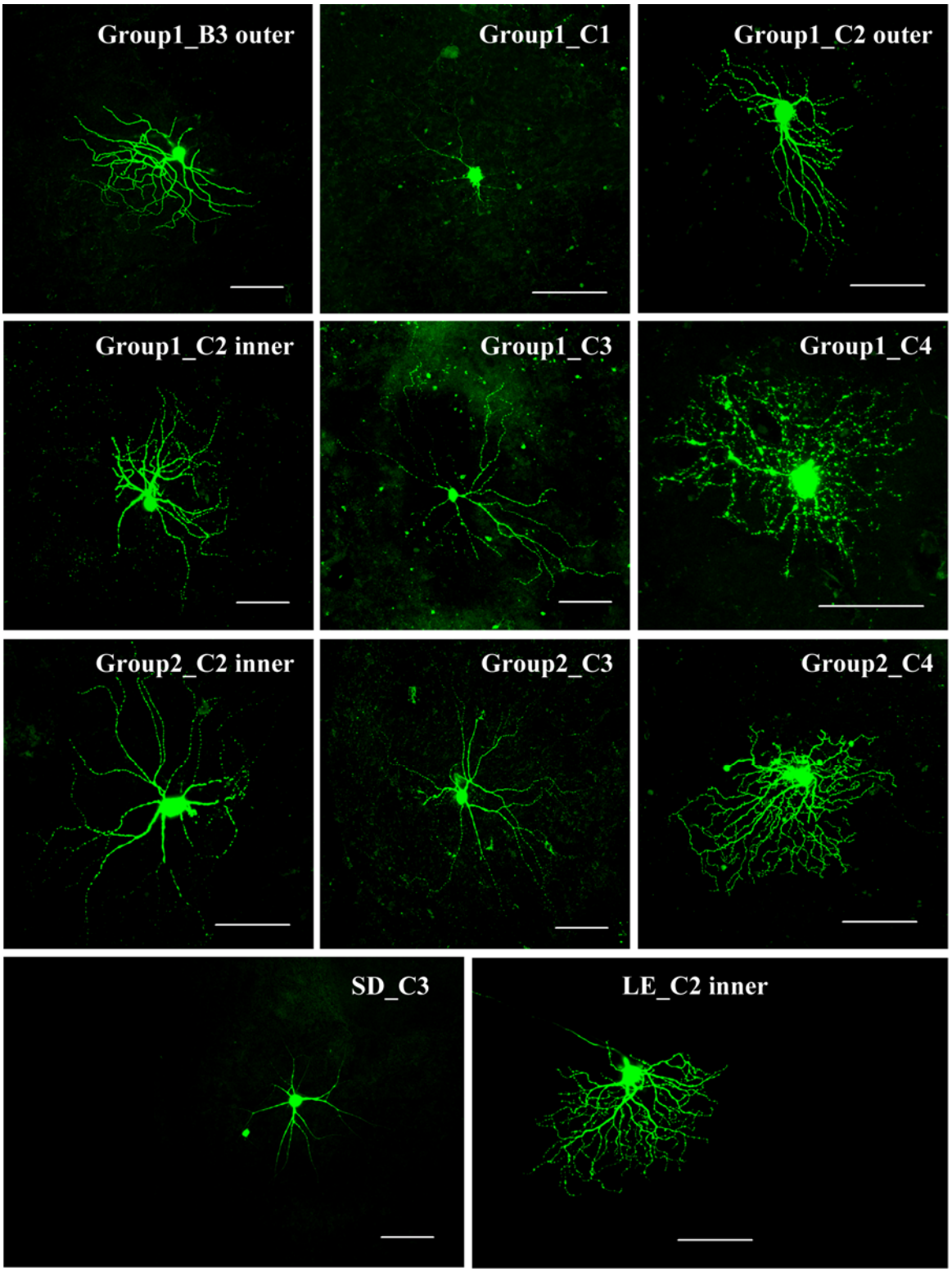

Figure S1 Confocal images of class RG_B and class RG_C in Group 1 RCS rats (B3, C1, C2 outer, inner, C3, and C4), Group 2 RCS rats (C2 inner, C3 and C4), SD rats (C3), and LE rats (C2 inner). Scale bar, 100 μm.